Computational Analysis of High Lift Generating Airfoils for Diffuser Augmented Wind Turbines

Aniruddha Deepak Paranjape[1], Anhad Singh Bajaj[1], Shaheen Thimmaiah Palanganda[1], Radha Parikh[1], Raahil Nayak[1], and Jayakrishnan Radhakrishnan[1]

1. Department of Aeronautical and Automobile Engineering, Manipal Institute of Technology, Manipal 576104, Karnataka, India.

Correspondence: Aniruddha Deepak Paranjape (aniruddha.deepak@learner.manipal.edu)

Abstract. The impetus towards sustainable energy production and energy access has led to considerable research and development in decentralized generators, in particular, diffuser augmented wind turbines. This paper aims to characterize the performance of a diffuser augmented wind turbines (DAWT), using high lift airfoils employing a three-step computational analysis. The study is based on computational fluid dynamics, and the analysis is carried out by solving the Unsteady Reynolds-averaged Navier-Stokes (URANS) equations in two dimensions. The rotor blades are modeled as an actuator disk, across which a pressure drop is imposed analogous to a three-dimensional rotor. We study the change in performance of the enclosed turbine with varying diffuser cross-sectional geometry. In particular, this paper characterizes the effect of a flange on the flow augmentation provided by the diffuser. We conclude that at the end of the three-step analysis, Eppler 423 showed the maximum velocity augmentation.

1 Introduction

Global energy demand is expected to more than double by 2050 due to the growth in population and development of economies (Gielen et al., 2019). Wind energy is emerging as an alternative renewable source for energy production. Presently, wind turbines are typically installed away from populated areas because of visual and noise regulations (Pedersen et al., 2014). This necessitates the transfer of electricity via grids over more considerable distances, increasing the levelized cost of electricity. While large wind turbines are placed where the wind topology is optimum, smaller wind turbines are locally built to supply power to meet the local energy demands.

A simplified modeling approach for the wind turbines is carried out, where the conventional horizontal axis wind turbine (HAWT), is modeled as an actuator disk (AD). The HAWT's can extract 59.3% of power available in the wind, in accordance to the Betz limit. DAWTs have the ability to increase the power extracted by the wind turbine by virtue of: increased mass flow rate through the rotor plane, improved wake mixing with the external flow, and lastly, improved performance even in cases where the flow may not be purely axial in nature.

The idea of a DAWT, also commonly referred to as a ducted wind turbine or shrouded turbine, was first explored by Lilley and Rainbird (Lilly and Rainbird, 1956). Since the early studies, numerous research based on empirical, computational and
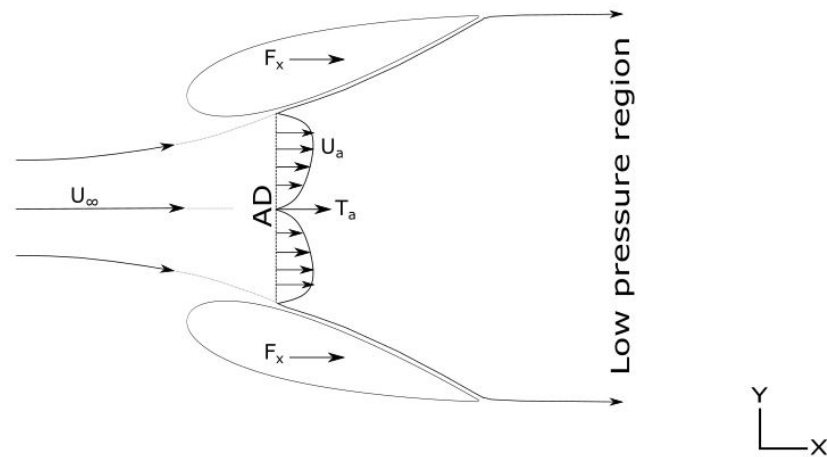
Figure 1. Schematic of a diffuser augmented wind turbine

experimental approaches have been conducted to investigate and optimize the efficiency of DAWT through various means (Alquraishi et al., 2019). By enclosing a diffuser around the turbine, the wake of the turbine blades is allowed to expand, resulting in a subsequent rapid drop in pressure aft of the diffuser. This, in turn, leads to an increase in the mass flow rate of the incoming free stream air, thereby increasing the efficiency of the system beyond the Betz limit. Through wind tunnel
5   testing, Igra (Igra, 1981) found that the power coefficient could be improved by 80% of that of a conventional wind turbine just by placing a diffuser over it. This phenomenon is termed as velocity augmentation. Abe and Ohya (Ohya et al., 2008), varied the diffuser open angle by adding a flange around the diffuser exit. The study showed that flanged diffusers, that is, an additional geometric modification to the shroud, can cause a larger wake expansion due to unsteady flow separated regions generated by the flange periphery. The mass flow rate is thus further increased by this geometric feature. Although there
10   is a significant amount of literature employing high-fidelity numerical modeling techniques applied to DAWTs, there is no preliminary analysis that may help potential manufacturers design diffusers with commonly available airfoil geometries.

    The present study uses high-lift airfoils to highlight a simplified simulation pipeline that may assist designers in assessing the suitability of a pool of airfoils while designing DAWTs or other decentralized wind energy generators. The use of high-lift airfoils in wind energy applications has been documented extensively in the literature. High lift airfoils improve the aerody-
15   namic efficiency (C_L/C_D) i.e lift to drag ratio, at low Reynolds number by virtue of a high lift coefficient with minimum drag penalties. In this study, we consider a two-dimensional flow field for the analysis, following studies conducted by Dighe (Dighe et al., 2018). The turbine is modeled as a two-dimensional AD and the separation effects and flow losses from the tips are assumed to be negligible. The study investigates the effect of camber, thickness, and a flange of a high-lift airfoil on a DAWT and

characterize their performance.The numerical analysis has been carried out by using the commercially available computational fluid dynamics (CFD) solver ANSYS® Fluent.

The remainder of this paper is organized as follows: Section 2 describes the AD modeling and presents the mathematical model used in the study. Section 3 discusses the simulation methodology and the validation of the computational study. Section 4 discusses the results of the study while section 5 summarizes the important results of the study.
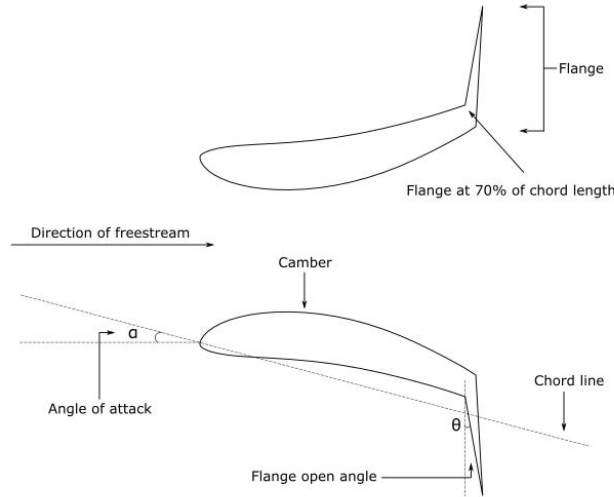
Figure 2. A schematic of the final geometry of the diffuser shape with all the parameters highlighted

2   Actuator Disk Modeling

The AD uses the mass and momentum conservation principles to balance the applied forces compared to the axial and tangential momentum equations that balance the applied forces on the real rotor blades. Although a two-dimensional simplification may not account for three-dimensional effects such as wake rotation and lateral flow, several studies have validated this approach .

The AD is considered to have an infinitesimal width, which exerts a constant thrust T_{AD}, per unit surface. The turbine or AD coefficient is given by:

$$C_{T_{AD}} = \frac{T_{AD}}{\frac{1}{2}\rho U_{\infty}{}^{2} S_{AD}}$$

where, ρ is the fluid density, U_{∞} is the free-stream velocity and S_{AD} is the surface area of the AD.

The thrust force T_{AD} force can be written as:

$$T_{AD} = S_{AD}(\Delta p)$$

where Δp is the pressure drop across the AD. δp, and ultimately $C_{T_{AD}}$ is input for the simulations as a constant, derived from experimental investigations conducted by (Tang et al., 2018). The current experimental configuration involves the consideration of an additional force created by the diffuser, T_{Duct}. Thus we can define $C_{T_{Duct}}$ as:

$$C_{T_{Duct}} = \frac{T_{Duct}}{\frac{1}{2}\rho U_\infty{}^2 S_{AD}}$$

The duct force F_{Duct} creates a mass flow across the AD plane.:

$$\dot{m} = \rho S_{AD} U_{AD},$$

Although a constant coefficient of thrust is assumed, the velocity across the AD is not uniform. The average AD velocity can be found by integrating the free-stream velocity over the defined surface area of the AD:

$$U_{AVG} = \frac{1}{S_{AD}} \int \frac{\partial U}{\partial x} dS$$

Using the above results we can define a power coefficient for the diffuser geometry with an AD of surface area S_a:

$$C_P = \frac{P}{\frac{1}{2}\rho U_\infty{}^2 S_{AD}} = \frac{U_{AVG}}{U_\infty} C_T$$

Therefore the total thrust force can be represented as a vectorial sum of the AD force T_{AD} and duct force T_{Duct}, given by:

$$T = T_{AD} + T_{Duct}$$

5   Thus the total thrust coefficient is given by:

$$C_T = C_{T_{AD}} + C_{T_{Duct}}$$

3   Computational Fluid Dynamics Methodology

3.1   Simulation Domain

To conduct the present study, ANSYS® and its constituent modules were used to generate, simulate, visualize and process the results. ICEM CFD®, ANSYS Inc., was used to generate the required mesh due to its significant control and flexibility over
10   the grid generation process. A C-Type topography was chosen as the computational domain, as highlighted in Figure 3, due to its easy generation and minimal skewness of the mesh in the near-wall condition. It also can accurately simulate the flow at various angles of attack. The geometry consists of two-dimensional planar airfoils symmetrically placed about the central axis along with a rotor modeled as an AD. Following the work of Dighe et al. (Dighe et al., 2019), the tip clearance has been fixed at 2.5% . The free-stream velocity is set as 6 m/s for the present study, and the flow is considered to be steady, uniform, and
15   incompressible for the airfoil chord length. While the simulated conditions are two dimensional, the conditions are sufficient
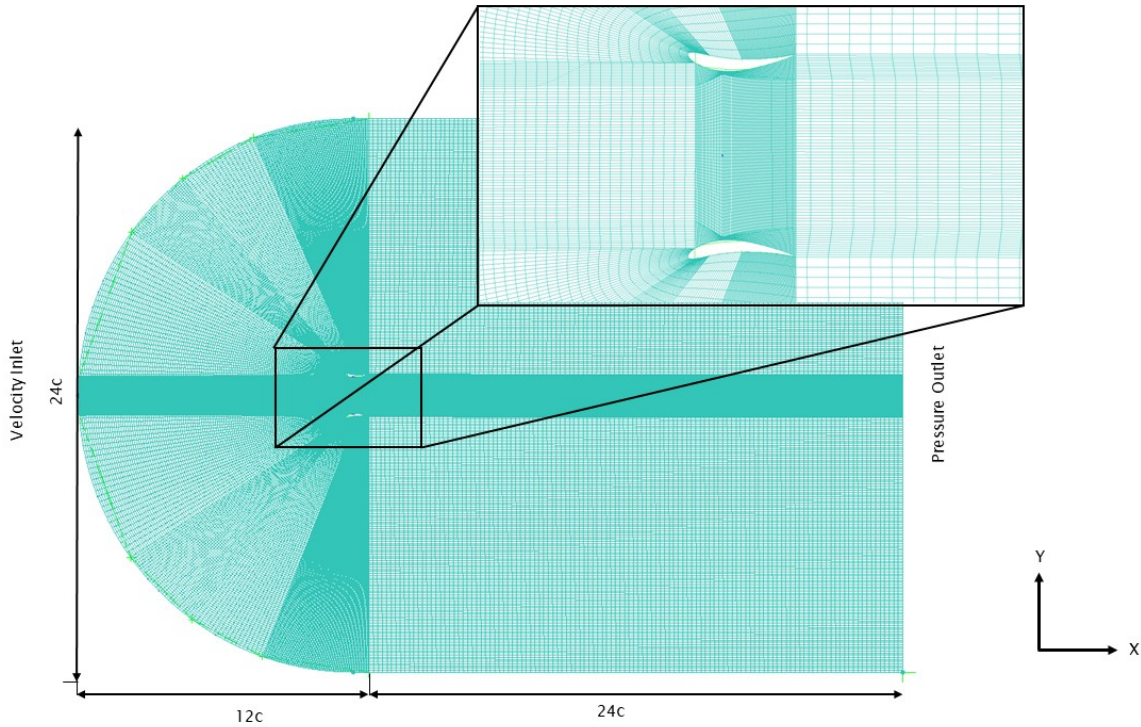
Figure 3. The C-Type topography computational grid

to gain enough insights due to the axisymmetric nature of the flow. For the given Reynolds number (Re = 400,000), the Y+ was maintained at a value less than 1, in order to calculate the wall spacing, therefore assisting the meshing process.

To properly model the viscous flows over the various diffuser configurations at turbulent Reynolds numbers, the Navier–Stokes equations are selected in the Cartesian coordinate system. Boundary conditions considered are: uniform velocity at the inlet, zero gauge static pressure at the outlet, no-slip walls for duct surfaces. The turbulence model used is the k-ω Shear Stress Transport (SST). The k-ω SST, which was developed by Menter (Menter et al., 1994), is a two equation robust model for turbulence growth and is one of the most widely used turbulence models. This is because the SST combines the use of $k - \omega$ in near wall flow and $k - \epsilon$ in free shear flow. This allows for a faster yet more accurate convergence of the solution.

ANSYS Fluent® was used as the flow solver, while CFD Post® and GNU Octave® were used to process the results.

3.2 Simulation Methodology

The present study assess the basic aerodynamic performance of high lift airfoils when applied to a DAWT geometry. Figure 4 highlights 12 airfoils chosen from 3 different airfoil families: Eppler, NACA, and Selig. The airfoils were selected based on their lift-drag ratio for the chosen Reynolds number. Formally, technique is called the "brute force method" (Dighe et al., 2018)

Figure 4. Selection of high lift airfoils across different families
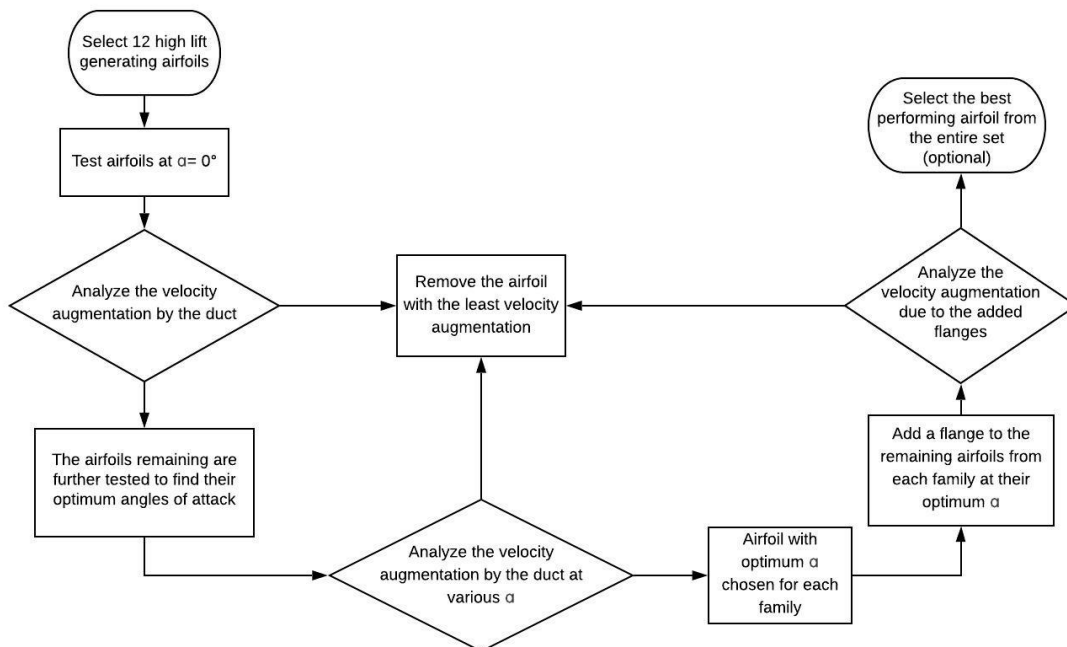
Figure 5. A flowchart that visualizes the simulation methodology and processes

The study was conducted in three stages. In the first stage, all airfoils were fixed at a constant angle of attack of $\alpha = 0°$ with respect to the horizontal. The angle of attack here corresponds to the area ratio. The area ratio is defined as the ratio of the diffuser exit area to the area of the AD (S_E/S_{AD}). The results obtained for each case were compared to the NACA 0012 test case. RANS equations were used in this analysis for maximum simplicity. Based on the results of the first stage of simulations, one airfoil was eliminated from each of the families on the basis of its velocity augmentation (Igra, 1981).

In the second stage, the angle of attack of the airfoils corresponding to their area ratios was varied and the end result was an optimized angle of attack for each of the families. After concluding simulations of the second phase, one airfoil from each family was eliminated based on its velocity augmentation again, leaving two best performing airfoils from each family. In the third stage, the six final airfoils were then analyzed at their optimum angles of attack and added with a 15° flange at the trailing edge at 70% of the chord to generate an unsteady low pressure region at the trailing edge, which in turn increases the mass flow rate at the AD.

A constant diffuser thrust co-efficient of $C_T = 0.767$ (Dighe et al., 2018) is maintained by keeping a constant pressure difference across the AD. The effects of varying the tip clearances on the duct performance are beyond the scope of this study.

3.3   Grid Validation and Independence Studies

A grid validation was conducted to verify the accuracy of the mesh, while a grid convergence study was conducted to determine the optimum mesh configuration without sacrificing the accuracy of the result.

Igra's (Igra, 1981) experimental wind tunnel set-up was replicated in the numerical domain to validate the generated mesh. Igra carried out numerous experiments during his research on diffuser augmented wind turbines. Of these, their work on the experimental set-up of the 'Circular Wing Shrouds' was considered a reference to validate our study. Analogous to the experimental set-up, the numerical domain uses the NACA 4412 airfoil, simulated in a planar diffuser configuration. The angle of attack of the airfoils was fixed at 2° and the area ratio was maintained at 1.84 for this configuration. Wall blockages and interference were ignored for the experimental set-up to avoid elaborate wind tunnel corrections. The inflow velocity was maintained at 6 m/s. The results were analyzed against experimental pressure distributions and forces.(Dighe et al., 2019) The final mesh generated using the ICEM CFD tool was akin to Igra's experimental results, thus proving the validity of the mesh.

Three meshes were used with a different number of nodes and elements in order to optimize the mesh in terms of simulation time. All the meshes had NACA 4412 as the airfoil and were simulated under similar conditions with an inlet velocity of 6m/s.

Table 1: Grid Convergence Study Results

Grid	Number of Elements	Velocity Output (m/s)
Coarse	4776	7.82
Medium	1752919	8.67
Fine	457512	8.76

The first mesh was coarse, with roughly 4627 nodes and 4776 elements in total, and took 2 minutes to converge. The coarse mesh produced an inferior result with a velocity of 7.82 m/s at the AD. The second mesh was a fine mesh with a total of 174246 nodes and 175291 elements. This mesh took about 10 minutes for the solution to converge and produced a better and more accurate result with a velocity of 8.67 m/s at the AD. The third mesh was even finer with a total of 456031 nodes and 457512 mesh elements. This mesh took 22 minutes for the solution to converge and produced a velocity of 8.76 m/s at the AD. The finest mesh differed by a 0.98% from the medium quality mesh. Thus the medium quality mesh with 174246 nodes and 175291 elements was chosen, as it was accurate with an added advantage of reduced computational time and power. The simulations were performed on a multi-core workstation desktop computer.

4   Results and Discussion

The following sections highlight the results of all the stages pertaining to the analysis. The airfoils were tested for different geometrical modifications as well as their aerodynamic performances. The under performing airfoils were removed from the analysis after each stage. The airfoils were evaluated at a constant diffuser thrust coefficient value $C_\mathrm{T} = 0.767$.
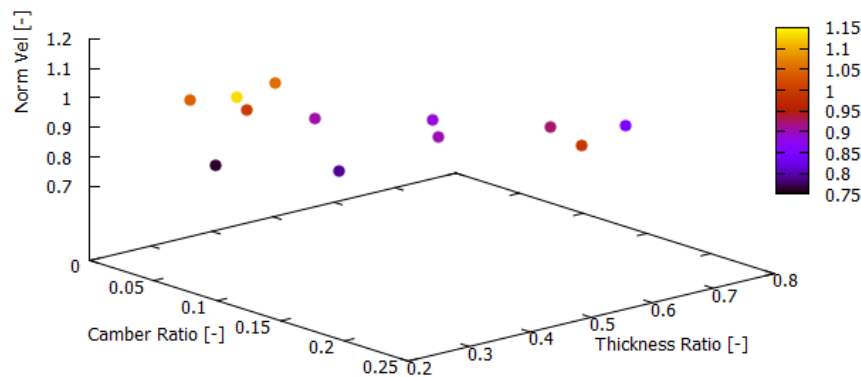
Figure 6. Effect of camber and thickness of the diffuser on the normalized velocity at the actuator disk

4.1   Stage 1: Constant α

All the simulations for the first stage were performed with an angle of attack $\alpha = 0°$ to assess the basic aerodynamic performance of the airfoils. Figure 6 expresses the variations of the camber, thickness, and diffuser velocities for the various airfoils maintained at $\alpha = 0°$. The camber (mc) and thickness (t) are represented as ratios, while the velocity at the AD has been normalized with respect to the free-stream velocity of 6 m/s. The camber ratio is defined as the maximum camber percentage to the

maximum camber location on the chord expressed as a percentage. The thickness ratio is defined as the maximum thickness percentage of the airfoil to the position on the chord at which the thickness is maximum. To assess the graph, the velocity has been presented with a iso chart. The colours represent the performance of the airfoils compared to the base case. From the results of the graph, three under performing airfoils, one from each family were eliminated. The airfoils eliminated were, the Selig S1221 with a $mc = 0.0997$, $t = 0.555$ and with a normalized velocity of 0.8863, Eppler E222 with a $mc = 0.0379$, $t = 0.3279$ and with a normalized velocity of 0.7616 and lastly NACA 63(2)-615 with a $mc = 0.1$, $t = 0.4$ and with a normalized velocity of 0.7885. Looking at Figure 6, it is clear that camber plays a crucial role in velocity augmentation, even among high lift airfoils, while the effect of thickness is not so pronounced. This can be attributed to the effect of curvature of the airfoil on the boundary layer. The boundary layer is subject to both, a curvature as well as a mean pressure gradient due to convex and concave upper and lower surface of a cambered airfoil. For the convex surface of the curvature, the angular momentum of the flow increases with an increase in curvature. As per the Rayleigh criterion, (Rayleigh, 1916) the increase in angular momentum causes a stabilizing effect on the flow resulting in lower skin friction coefficient. Thus the direct effect of camber can be seen in higher velocity augmentation at the AD, resulting in a higher C_{P} as per the classical definition of the power coefficient. This also highlights the strong correlation between the camber and the velocity augmentation at the AD, similar to previous studies done in DAWT.

4.2 Stage 2: Varying α to find the optimum angle for maximum velocity augmentation

For the second stage analysis, the best performing airfoils were taken from the results of stage one, which were based on the velocity augmentation at the AD. The angles of attack of the airfoil were varied, wherein the area ratios associated with it also changed, while the C_{T} was maintained at 0.767. Here the angles of attack were varied from $\alpha = 0°$ to $\alpha = 12°$ in steps of 4°, and subsequently by 1° till $\alpha = 20°$. For the initial variations of up to 12°, the flow remained attached to the surface of the airfoil. As the angle of attack was increased, an upward trend was noted in the velocity at the AD. This is a consequence of an increase in the mass flux of the wind as a result of the changing area ratios. Beyond a certain angle of attack and area ratio, a flow separation was observed on the pressure side of the airfoil, which was found to be detrimental to the velocity augmentation of the airfoil. Thus, there was an optimum angle of attack and area ratio where there was maximum velocity augmentation. Based on the results of the simulation, the optimum angle for Eppler, NACA and Selig was found to be $\alpha = 15°$, $\alpha = 14°$ and $\alpha = 18°$, respectively. Based on the criteria of velocity augmentation at the AD, the study was taken forward by eliminating the NACA 64A410, S1221, and E1210 airfoils which registered the least velocity augmentation in stage two.

4.3 Stage 3: Effects of a Flange

A third and final stage was conducted by adding a flange at 70% of the airfoil chord at an open angle of 15°, as per the study conducted by El-Zahaby et al. (El-Zahaby et al., 2016). Figure 2 highlights the final geometry of the diffuser shape along with the various parameters that define the design geometry. It was observed that there was a significant increase in the velocity at the AD after the addition of the flanges. This velocity increase can be attributed a region of separated flow this is generated due to the presence of the flange. The separated flow produces a region of unsteady low pressure which increases the mass flux of

wind at the AD. Figure 7 consists of the velocity contours of the final set of airfoils a) NACA 2411, b) NACA 4412, c) Eppler 59, d) Eppler 423, e) Selig 1210, f) Selig 1223. The vortices are easily visualized in Figure 7 along with the flow separation due to flange.
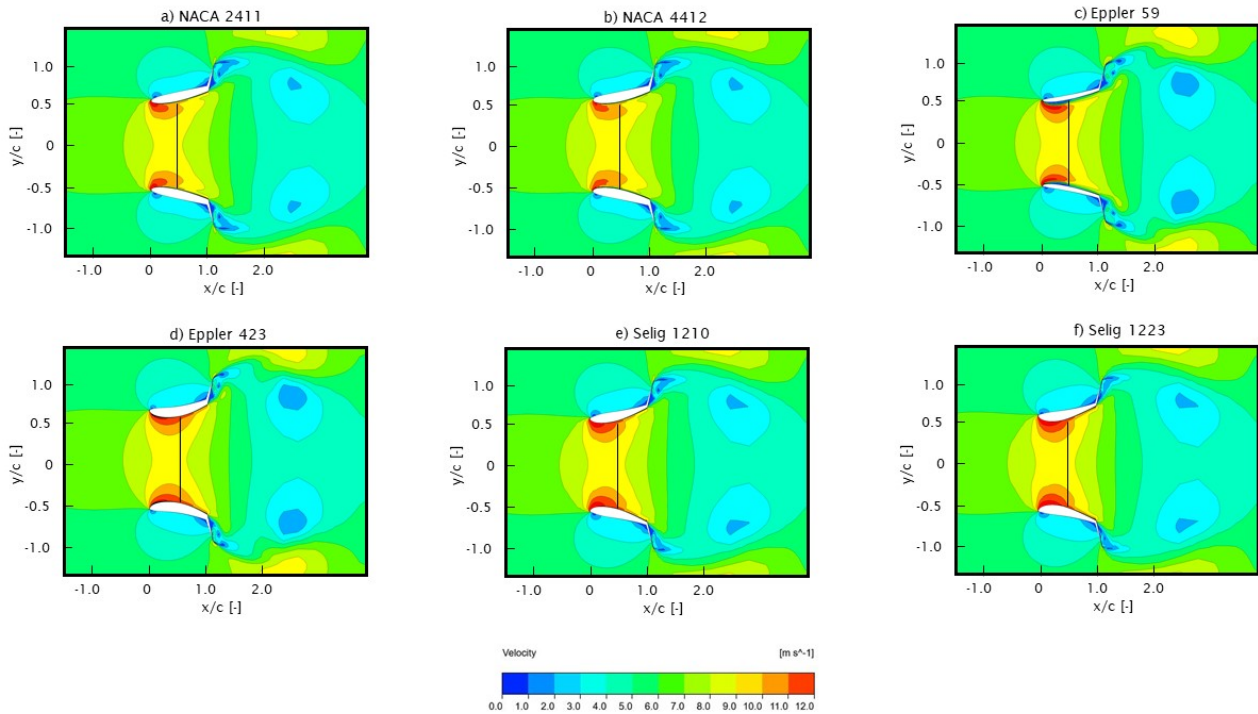
Figure 7. Velocity contours of the streamwise normalized velocity. The results depict performance of the stage three airfoils at $C_T = 0.767$

According to the classical definition of the power coefficient, the C_P is affected by the velocity of the flow at the AD. The power co-efficient is an important parameter that is used to determine the diffuser performance. Figure 8 is used to visualize the effect of the thickness ratio and camber ratio on the C_P in a 3D space. To assess the graph, the C_P has been presented with a colour chart. NACA4412, S1223, and E423 are the best performing airfoils from each of the respective families in terms of velocity augmentation and C_P, with a velocity output of 9.21 m/s, 9.41 m/s, and 9.43 m/s respectively. Overall, Eppler 423 showed the maximum velocity augmentation and C_P among all the 12 airfoil geometries that were considered.

For the best performing airfoil, the thrust coefficient C_T was varied, and the resulting velocity at the AD was normalized with the free-stream velocity. Figure 9 shows an almost linear relation between the parameters. Increasing the C_T results in a reduction of the velocity augmentation; this phenomenon can be compared to increasing the blockage to the flow by virtue of an increase in resistance. This is in agreement with other work performed in DAWT and DAWT theories. The current simulations are performed with a moderate value of C_T. The exact effects of the C_T and tip clearance are out of the present scope of the study, but can be the subject matter of another study.
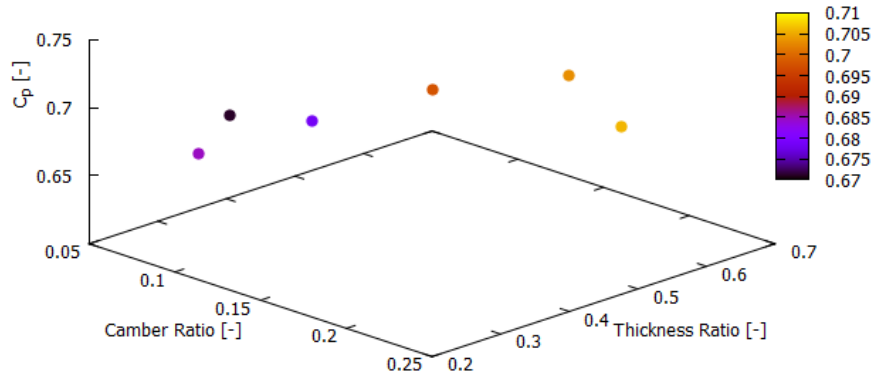
Figure 8. Effect of camber and thickness of the diffuser on the C$_P$ for the airfoils in the third stage
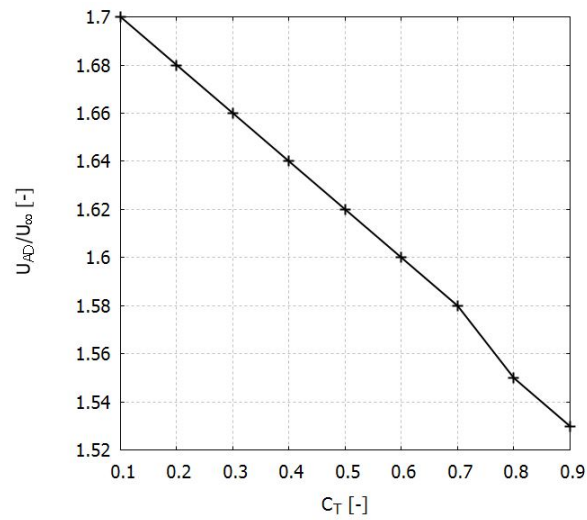
Figure 9. The result depicts the effect of varying the C$_T$ on the normalized velocity at the actuator disk

5 Conclusions

The present study uses high-lift airfoils to highlight a simplified simulation pipeline that may assist designers in assessing the suitability of a pool of airfoils while designing DAWTs or other decentralized wind energy generators. The use of high-lift airfoils in wind energy applications has been documented extensively in the literature. High lift airfoils improve the aerodynamic efficiency (C_L/C_D) i.e lift to drag ratio, at low Reynolds number by virtue of a high lift coefficient with minimum drag penalties. The diffusers, made up of the 12 high-lift airfoils, were subject to evaluation in three different stages. In the first stage, the area ratio was kept constant by maintaining the $\alpha = 0°$. Based on the velocity augmentation, the best performing airfoils were tested by varying their area ratios and their corresponding angles of attack in stage two. An optimum angle of attack with maximum velocity augmentation was found at the end of stage two. A final, third stage was performed by adding a flange of $15°$ to the airfoils. Based on the results of velocity augmentation and C_P, it was concluded that E423 was the best performing airfoil. The detailed effects of tip clearance and C_T on the effects of diffuser performance can be a subject of a future study.

6 Appendix A

Nomenclature

α Angle of attack of the airfoil [°]

5   ρ Density of air [kg/m^3]

AD Actuator Disk

c Diffuser chord length [m]

C_P Power coefficient of the AD [-]

$C_{T_{AD}}$ Thrust coefficient of the AD [-]

10   $C_{T_{Duct}}$ Thrust coefficient of the Duct [-]

C_T Total thrust coefficient of the AD model [-]

$DAWT$ Diffuser Augmented Wind Turbine

$HAWT$ Horizontal Axis Wind Turbine

mc Camber ratio [-]

15   S_{AD} Reference area of the AD [m^2]

S_E Area of the exit of the diffuser [m^2]

T Total thrust force of the diffuser [N]

t Thickness raito [-]

T_{AD} Thrust force on the AD [N]

20   T_{Duct} Thrust force on the diffuser [N]

U_{AD} Velocity at the AD plane [m/s]

U_{AVG} Average velocity at the AD plane [m/s]

U_∞ Free-stream velocity [m/s]

x Variable value vector parallel to the free-stream direction [-]

y Variable value vector normal to the free-stream direction [-]

Author contributions. ADP wrote the bulk of the paper, performed the CFD simulations and post-processed the results. ASB performed CFD simulations and contributed to writing and reviewing the paper. STP modeled the geometries and contributed significantly in writing the paper. RP modeled the geometries. RN performed CFD simulations and helped set up the CFD simulations. JR helped formulate ideas through group discussions.

Competing interests. The authors declare that they have no conflicting or competing interests.

7 References

Alquraishi, B. A., Asmuin, N. Z., Mohd, S., Abd Al-Wahid, W. A., Mohammed, A. N. (2019). Review on Diffuser Augmented Wind Turbine (DAWT). International Journal of Integrated Engineering, 11(1) Aly, M., El-Zahaby, Kabeel, A.,E., Elsayed., S.,S., Obiaa, M.,F.,: : CFD analysis of flow fields for shrouded wind turbine's diffuser model with different flange angles, Alexandria Engineering Journal (2016), https://doi.org/10.1016/j.aej.2016.08.036, 2017.

A. Aranake and K. Duraisamy: Aerodynamic optimization of shrouded wind turbines, Wind Energ. (2016) DOI: 10.1002/we.2068

Dighe,V. V., Oliveira,G.de.: On the effects of the shape of the duct for ducted wind turbines, AIAA SciTech Forum. 2018.

Dighe,V. V., Oliveira,G.de., Avallone,F., van Bussel G.J.W.: Towards improving the aerodynamic performance of a ducted wind turbine: A numerical study. Journal of Physics: Conf. Series, :10.1088/1742-6596/1037/2/022016, 2018. 16

Dighe, V., Suri, D., Avallone, F., and van Bussel, G.: Ducted wind turbines in yawed flow: A numerical study, Wind Energ. Sci. Discuss., https://doi.org/10.5194/wes-2019-62, in review, 2019.

Ghenai,C., Salameh, T., Janajreh, I.: Modeling and Simulation of Shrouded Horizontal Axis Wind Turbine Using RANS Method. JJMIE. 11. ISSN 1995-6665. 2017.

Gielen, D., Boshell, F., Saygin, D., Bazilian, M. D., Wagner, N., and Gorini, R.: The role of renewable energy in the global energy transformation, Energy Strategy Reviews, 24, 38–50, 2019.

Igra, O.: Research and development for shrouded wind turbines, Energy Cont. Momt Vol. 21. pp. 13 to 48, https://doi.org/10.1016/0196-8904(81)90005-4, 1981

Lilley, G.,M., Rainbird, W., J,: A preliminary report on the design and performance of ducted windmills Report No. 102, April, 1956.

Menter, F., R.,: Two-Equation Eddy-Viscosity Turbulence Models for Engineering Applications, AIAA JOURNAL Vol. 32,No. 8, August 1994

Mikkelsen, R. F.: Actuator Disk Methods Applied to Wind Turbines, Kgs. Lyngby, Denmark: Technical University of Denmark (DTU). MEK-FM-PHD, No. 2003-02, 2004

Ohya, Y., Karasudani, T., Sakurai, A., Abe, K-I., Inoue, M.:Development of a shrouded wind turbine with a flanged diffuser. Journal of Wind Engineering and Industrial Aerodynamics, 96(5), 524-539. https://doi.org/10.1016/j.jweia.2008.01.006, 2008.

Radhakrishnan, J., and Suri, D.: Design and Optimisation of a Low Reynolds Number Airfoil for Small Horizontal Axis Wind Turbines, IOP Conference Series: Materials Science and Engineering. Vol. 377. No. 1. IOP Publishing, doi:10.1088/1757-899X/377/1/012053, 2018

Suri, D.: Design of an Optimized Inlet Shroud for a Flanged Diffuser, 10.31224/osf.io/2qb6r, 2019.

Tang, J., Avallone, F., Bontempo, R., van Bussel GJW, Manna, M.:Experimental investigation on the effect of the duct geometrical parameters on the performance of a ducted wind turbine. J Phys Conf Ser. 2018;1037(2):022-034.

Rayleigh, R.:On Convection Currents in a Horizontal Layer of Fluid When the Higher Temperature Is on the Underside. Philosophical Magazine, 32, 529-546. http://dx.doi.org/10.1080/1478644160863560, 1916

Pedersen, E., Waye, K. P.:Perception and annoyance due to wind turbine noise—a dose–response relationship, https://doi.org/10.1121/1.181
2004